

Article

Understanding the Planform Complexity and Morphodynamic Properties of Brahmaputra River in Bangladesh: Protection and Exploitation of Riparian Areas

Shiblu Sarker ^{1,*} , Tanni Sarker ² , Olkeba Tolessa Leta ¹ , Sarder Udoy Raihan ³ , Imran Khan ⁴ and Nur Ahmed ¹ 

¹ Bureau of Watershed Management and Modeling, St. Johns River Water Management District, Palatka, FL 32177, USA

² School of Planning, Design and Construction, Michigan State University, East Lansing, MI 48824, USA

³ Bangladesh Water Development Board, Dhaka 1215, Bangladesh

⁴ Institute of Water Modelling (IWM), Dhaka 1230, Bangladesh

* Correspondence: shiblu.buet@gmail.com

Abstract: The Brahmaputra River (BR) is a heavily braided river, due to various intricate paths, high discharge variability and bank erodibility, as well as multi-channel features, which, in turn, cause huge energy dissipation. The river also experiences anastomosing planform changes in response to seasonal water and sediment waves, resulting in a morphology with extreme complexity. The purpose of this study was to provide detailed and quantitative insights into the properties of planform complexity and dynamics of channel patterns that can complement previous studies. This was achieved by investigating the applicability of the anastomosing classification on the Brahmaputra river's planform, and computing disorder/unpredictability and complexity of fluctuations using the notion of entropy and uniformity of energy conversion rate by the channels, by means of a power spectral density approach. In addition, we also evaluated their correlation with discharge as a dynamic imprint of river systems on alluvial landscapes, in order to test the hypothesis that river flow may be responsible for the development of anastomosing planforms. The analysis suggests that higher discharge values could lead to less complex planform and less fluctuations on the alluvial landscape, as compared to lower discharge values. The proposed framework has significant potential to assist in understanding the response of complex alluvial planform under flow dynamics for the BR and other similar systems.

Keywords: anastomosing; Fourier transform; power spectral density; sample entropy; approximate entropy



Citation: Sarker, S.; Sarker, T.; Leta, O.T.; Raihan, S.U.; Khan, I.; Ahmed, N. Understanding the Planform Complexity and Morphodynamic Properties of Brahmaputra River in Bangladesh: Protection and Exploitation of Riparian Areas. *Water* **2023**, *15*, 1384. <https://doi.org/10.3390/w15071384>

Academic Editor: Vlassios Hrisanthou

Received: 24 February 2023

Revised: 24 March 2023

Accepted: 28 March 2023

Published: 3 April 2023



Copyright: © 2023 by the authors. Licensee MDPI, Basel, Switzerland. This article is an open access article distributed under the terms and conditions of the Creative Commons Attribution (CC BY) license (<https://creativecommons.org/licenses/by/4.0/>).

1. Introduction

The Brahmaputra River (BR) is often characterized as a braided river due to its complex networking of channels, branches and bars, including high sediment loading, and significant variability in discharge and gradients [1–3]. The high variability in discharge and sediment loading from the Brahmaputra River Basin (BRB) are the main factors responsible for significant erosion–deposition processes [4–8], which also initiate the complex network along with bar dynamics. The morphological processes, such as soil erosion, deposition, channel movement and irregular planform structure, combined with significant stream power variability are critical for understanding such kinds of river systems [9–12]. As such processes frequently occur in braided river systems, they cannot be measured over a short period of time. Several previous studies have been conducted to better understand the planform process of braided rivers, that include the following: flume experiments [13–16], numerical modeling [17,18], satellite-based remote sensing products [19–24], and modern technology, such as digital photogrammetry and laser altimetry [25–28]. However, these

previous studies have lacked detail analysis of morphodynamics and planform complexity of channels especially for braided river systems.

Since the BR is one of the world's most braided and sand-bedded river systems, and is ranked fifth in terms of its annual flow, it is an ideal river system for studying river planform complexity and randomness [29–33]. In addition, the BR system experiences a unique characteristic in terms of inter-seasonal variability of flow–sediment loading and morphological processes [32,34–36]. Furthermore, a series of large floods and major tectonic activity in the BR system have resulted in a complex morphodynamic environment [32,37,38]. The banks of the BR have been heavily eroded, including frequent changes in the channel courses. Such morphological dynamics and processes have tremendous impacts on the functioning of the riverine ecosystem and on the approximately 30 million people that live along the river banks [39,40]. Therefore, detailed analysis of the morphodynamics of the BR system, such as identifying the stable and unstable parts of the river's reaches, is of interest to enhance our understanding and so as to implement appropriate and sustainable mitigation measures for the system.

As previously discussed, the high variability of discharge and sediment loading from the BRB to the BR system are most likely responsible for significant erosion–deposition processes [4–7], which also initiate formation of complex network systems and dynamics along riverine and alluvial areas. Due to the high variability of discharge and sediment loading, and complex morphodynamics of the BR system, performing an analysis of the spatio-temporal variability of the planform and dynamic forcings are of interest for a better understanding of the BR system. In addition, it is also critical to investigate the effect of bar dynamics on the morphological reorganization combined with planform complexity. Our objective was to generate generic insights into the properties of planform complexity and dynamics of the channel patterns that complement previous studies. We address this by computing the planform complexity and randomness using complex network metrics and a theoretical approach that shed some light on understanding the dynamic behavior of the river and help to minimize the gap between previous studies on braided rivers.

2. Study Area

The Brahmaputra River Basin (BRB) outspreads in Bangladesh (5.47%), India (36.11%), Nepal (0.13%), Bhutan (7.20%), Tibet and China (51.08%), as shown in Figure 1. Geographically, the basin is situated between $82^{\circ}1' E$ and $97^{\circ}46' E$, and $22^{\circ}27' N$ and $31^{\circ}27' N$. Bounded by the Himalayas on the northwest, Tibetan plateau on the north, Ganges basin on the west, Meghna basin on the south, and Meghalaya subtropical forests on the south-east, the BRB drains an area of approximately $543,462 \text{ km}^2$ [41]. In India's territory, the basin stretches over the states of Arunachal, Sikkim, Assam, West Bengal, Nagaland, Meghalaya and Manipur, of which Arunachal represents the highest distribution of the drainage area (41.24%), followed by Assam (37.07%).

The BRB is characterized by an irregular shape with a maximum east–west length of 1540 km and a maximum north–south width of 835 km [41]. The BR originates from Kailash (the great glacier mass of Chema-Yung-Dung) of the Himalayas, at an elevation of about 5150 m, and flows for about 2900 km through Tibet, China, India and Bangladesh, eventually confluent with the Ganges River. In China, the BR is known as the Yarlung Tsangpo, that flows east at an average elevation of 4000 m above *MSL*. Flowing eastward for a length of about 1130 km, the Yarlung Tsangpo River bends around Mt. Namcha Barwa, thereby forming the Yarlung Tsangpo Canyon, the deepest in the world. The river then turns towards the south, entering the Arunachal Pradesh State of India, wherein it flows for about 35 km and joins the Dibang and Lohit Rivers. From this confluence, the river becomes very wide and is referred as the Brahmaputra River, where the average slope of the river drastically reduces to 0.1 m/km compared to 2.82 m/km in Tibet, China [42]. A few more tributaries join the main course of the river later, both on the left and right banks, before the river enters Bangladesh. At the border of Bangladesh, the river curves to the south and south–east directions. The branch curving towards the south continues as the Jamuna

and flows for a length of about 240 km to its confluence with the Lower Ganges at Aricha, locally called Padma. The Brahmaputra River has an average annual flood peak flow of 60,000 m³/s at Bahadurabad of Bangladesh (around 150 km upstream of the confluence), with the monsoon flood typically occurring between July and August. When the bank of the BR is full, the discharge volume is reduced to approximately 44,000 m³/s. The lowest discharge, approximately 5000 m³/s, occurs in January and February. The discharge is quite steady during January to February but steadily increases from March to June and then gradually declines from September to December [7,43,44].

This study was accomplished by evaluating a huge section of the Brahmaputra River from geographical and temporal points of view. Therefore, we limited our focus to the Brahmaputra River’s reach within the Bangladesh territory, as shown in Figure 2.

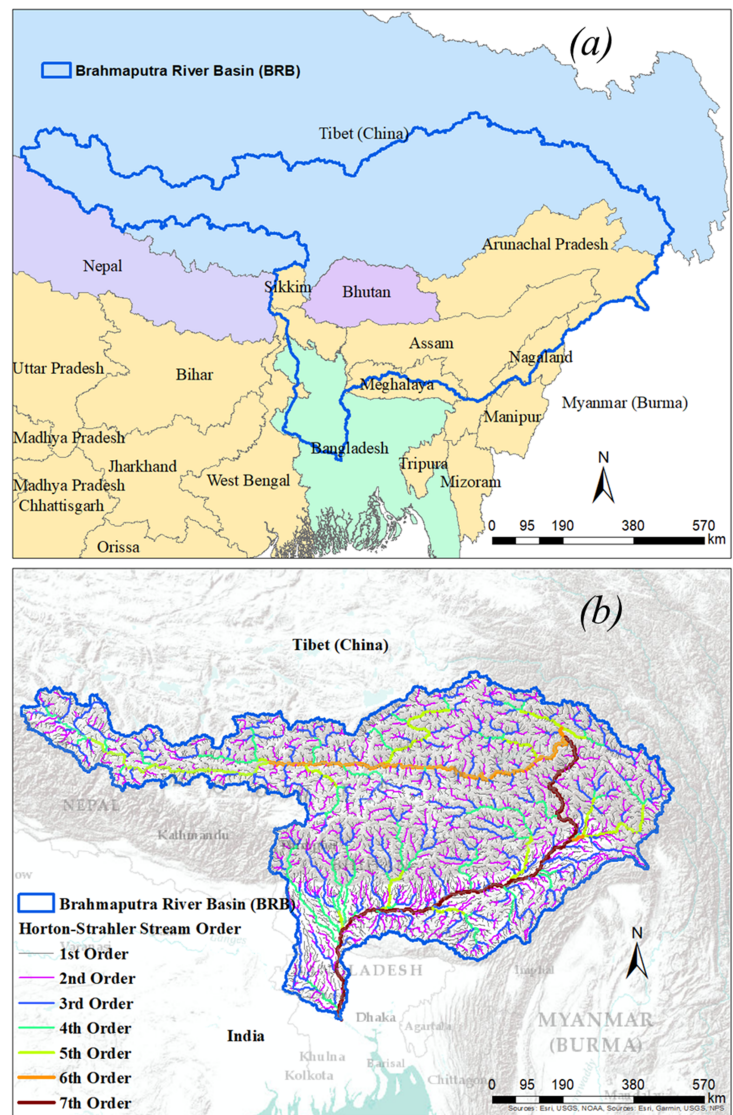


Figure 1. (a) The Brahmaputra River Basin (BRB) extent and (b) one-dimensional river network extracted from [4,6,8] for the BRB.

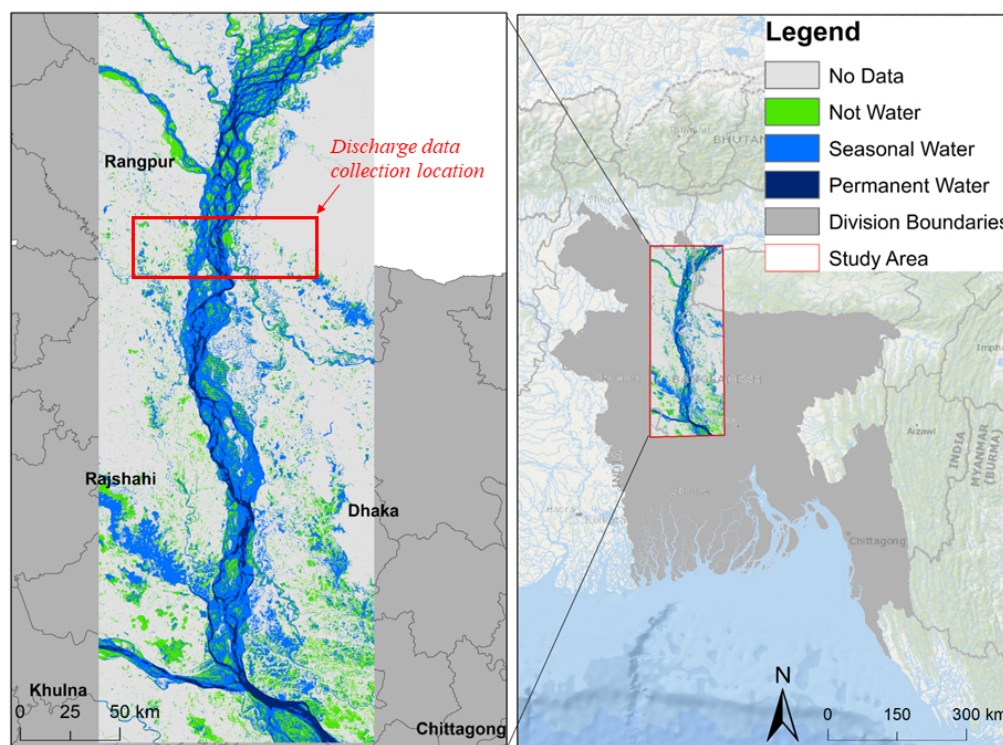


Figure 2. Brahmaputra River study region. The location of discharge data collection is depicted in red.

3. Methods

3.1. The Anastomosing River Principle

Anastomosing rivers usually occur in alluvial plains, where low energy and dense channel vegetation conditions persist, including floodplain geomorphology and structure. Based on the pattern of the channels, anastomosing rivers can be classed as having straight, meandering, and braided shapes. Avulsions or structures that divert flow and create a new channel pattern in the floodplain are commonly employed to build anastomosing rivers [3]. Such systems experience simultaneous multiple floodplain channels erosion, especially when bypasses are developed and older channel belt segments remain active for an extended period of time. The first type of anastomosis affects the entire floodplain, whereas the second type only affects a portion of it. Protracted anastomosis is generally caused by channel belt aggradation and/or channel capacity degradation as a result of in-channel deposition, both of which are facilitated by a low floodplain gradient [3]. There are numerous other reasons, including climate-related factors, such as catastrophic flood events, in-channel aeolian dunes or rapid base level rises. Based on the available information about the BR, the river can be considered an anastomosing river, which provides an ideal setting for hypothesizing its planform and characterizing its anastomosing nature [5]. Therefore, applying complex network theory is crucial to gain better understanding of the physical processes occurring in the alluvial landscapes of the river. In this study, the Brahmaputra River's high complexity permits us to hypothesize in regard to the meandering and braided categories, and, particularly, in regard to the anastomosing category of the river.

3.2. Channel Network Delineation

Several scholars have investigated the Brahmaputra River in detail over a long period of time. For this study, the data acquisition and the processing to delineate the channel network of the BR were performed using the online code editor of the Google Earth Engine (GEE). GEE provides free access to cloud-based large-scale geospatial data sets and analysis [45]. We used image collections or data stack, all available from the USGS Landsat

surface reflectance products (TM, ETM+, OLI) and acquired during the dry season. We used yearly data for the period from 1987 to 2020. The dry periods were selected between 1 October and 30 December for each year. *GEE* was also used to intersect all the dry images within the study area and to combine them per year, creating a cloud-free yearly composite scene, as shown in Figure 3. We deployed ArcGIS to delineate the channel network of the BR, based on the annual seasonal and permanent water pathways.

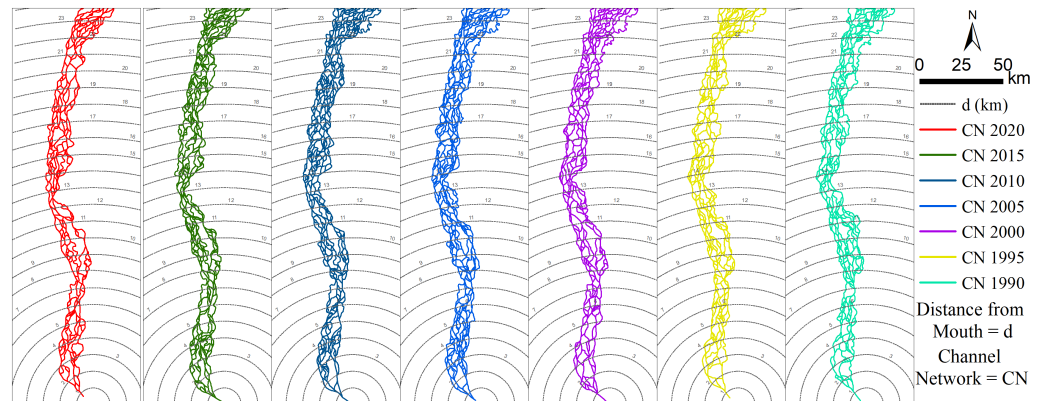


Figure 3. Delineation of the channel network for seven selected years from 1987 to 2020, based on the dry season of the Brahmaputra River.

3.3. Anastomosing Function

In this study, we proposed a series, called the Anastomosing Function (*AF*), to capture the one-dimensional spatial arrangement of the two-dimensional complex network planform of the Brahmaputra River. The River Network Width Function (*RNWF*) is commonly used by geomorphologists to characterize a river basin [4,46]. A *RNWF* is a one-dimensional function that summarizes the river network's two-dimensional branching structure [47]. Moreover, it displays the distribution of travel distances within the network, as well as the probability distribution of travel duration under the assumption of constant flow velocity [47]. While *RNWF* represents the number of channelized pixels or number of crossed channels that have the same distance from the basin outlet, the distances are measured along the flow path [4,46]. We developed the concept of *AF*, based on the similar notion of the *RNWF* method previously used in many studies (see details in [4,46]). Similar to the *RNWF* method, the *AF* computes the number of crossed channels as a function of the distance from the mouth of the Brahmaputra River, but not from the basin outlet (see details in [5]). Furthermore, since measuring distance along the flow path (longest channel) of braided rivers is very challenging, we, instead, proposed and adopted a radial distance method, with a constant interval from the mouth of the river, to generate *AF*. We applied this from the mouth of the Brahmaputra River where it meets the Ganges River. Mathematically, *AF* can be expressed as:

$$AF(d) = \#[\text{Channelized } I : d \leq R(I) \leq d + \delta d] \quad (1)$$

where $R(I)$ is the flow distance of channel intersection I from the mouth and δd is the scale of refinement. Usually, the distance d is normalized by R and $AF(d)$ is normalized by the total number of channel intersections rendered by their density. For a given anastomosing network topology, $AF(d)$ can be viewed as a stochastic process indexed by the distance d (similar to width function [47]). The concept of distance d was normalized by R for the seven selected years from 1990 to 2020, as depicted in Figure 3.

3.4. Discharge Data

We collected yearly maximum discharge data of the BR for the period from 1987 to 2020 at the Bahadurabad gauging station of Bangladesh, from the Bangladesh Water Development Board (*BWDB*), which serves as the national hydrological data provider of

Bangladesh (<https://bwdb.portal.gov.bd/>, accessed on 3 November 2021). The collected data is shown in Figure 4. The discharge data in this study was used as a dynamic imprint of the river to understand its relationship with planform complexity and fluctuation. Specifically, we tested our hypothesis using yearly maximum, mean wet, and mean dry discharge values as dynamic variables (see Figure 4).

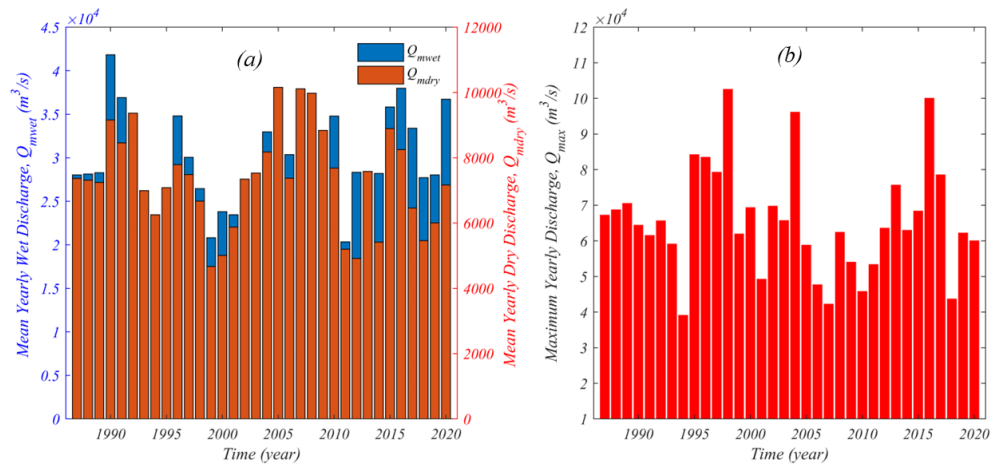


Figure 4. (a) Extracted mean yearly wet and dry discharge data and (b) Yearly maximum discharge data of the BR from 1987 to 2020.

3.5. Entropy

The entropy of a data series is a measure of its unpredictability. When moment statistics, such as mean and variance, are unable to distinguish between series, entropy is commonly utilized. Entropy measures the amount of information contained in a signal based on the probability of each signal value. In other words, entropy quantifies the degree of uncertainty associated with the occurrence of events across a space or time domain [48]. It can be expressed as:

$$En = - \sum_{i=1}^N p[af(i)] \log p[af(i)] \tag{2}$$

where $p[af(i)]$ is the probability of $af(i)$. The value $af(i)$ denotes each data value and N is the sample size of the corresponding signal represented by a vector $S = af(1), af(2), \dots, af(N)$.

Approximate Entropy and Sample Entropy are two other algorithms commonly used to determine the regularity of data series, based on the appearance of patterns [49].

3.5.1. Approximate Entropy

Approximate Entropy ($ApEn$) is a form of Shannon Entropy and its calculation requires a large amount of data in a series. Steve M. Pincus created a statistical method to overcome the limitations of moment statistics by modifying an exact regularity statistic [50,51]. It was initially developed for the analysis of medical time series data, but its applications have since been expanded to other fields [4,50–52]. In this study, we were interested to compute $ApEn$ as a measure of disorder of a data series: for example, a data series S containing N data values, $S = af(1), af(2), \dots, af(N)$. From this data, a series of vectors can be constructed as:

$$AF(1) = af(1), af(2), \dots, af(m) \tag{3a}$$

$$AF(2) = af(2), af(3), \dots, af(m + 1) \tag{3b}$$

$$\dots \tag{3c}$$

$$AF(N - m + 1) = af(N - m + 1), af(N - m + 2), \dots, af(N) \tag{3d}$$

The distance between two vectors $AF(i)$ and $AF(j)$ can be defined as the maximum difference in their respective corresponding elements.

$$\mathcal{D}[AF(i), AF(j)] = \max_{k=1,2,\dots,m} (|AF(i+k-1), AF(j+k-1)|) \tag{4}$$

where $i = 1, 2, \dots, N - m + 1$ and $j = 1, 2, \dots, N - m + 1$ and N are the numbers of data points in the series. For each vector $AF(i)$, a measure that describes the similarity between the vector $AF(i)$ and all other vectors $AF(j)$ $j = 1, 2, \dots, N - m + 1, j \neq i$ can be constructed as:

$$C_i^m(r) = \frac{1}{(N - m + 1)} \sum_{j \neq i} \theta(r - \mathcal{D}[AF(i), AF(j)]) \tag{5}$$

where

$$\theta(af) = \begin{cases} 1, & af \geq 0 \\ 0, & af < 0 \end{cases} \tag{6}$$

In our context, the value of θ was 1. The symbol r specifies a filtering level and is related to the standard deviation of the series. Finally, $ApEn$ can be calculated by the following equation:

$$ApEn(m, r) = \mathcal{O}^m(r) - \mathcal{O}^{m+1}(r) \tag{7}$$

where

$$\mathcal{O}^m(r) = \frac{1}{(N - m + 1)} \sum_i \ln[C_i^m(r)] \tag{8}$$

The application of Approximate Entropy ($ApEn$) on the $AF(d)$ data is shown in the following flow chart (Figure 5).

3.5.2. Sample Entropy

Sample Entropy ($SampEn$) is a modified form of Shannon entropy that is used to evaluate the complexity of physical time series signals and physical states. While $SampEn$ is a measure of complexity, which is similar to approximate entropy, it excludes self-similar patterns [51,53].

Both $ApEn$ and $SampEn$ algorithms are based on the conditional probabilities (see details in [54]), and the first two steps (3) and (4) are similar to $ApEn$, as shown in Figure 5. After the second step, $SampEn$ is calculated for each template vector using Equation (9):

$$B_i^m(r) = \frac{1}{(N - m - 1)} \sum_{j=1, j \neq i}^{N-m} \text{number of times that } \mathcal{D}[AF(j) - AF(i)] < r \tag{9}$$

Then, summing all template vectors can be written as Equation (10):

$$B^m(r) = \frac{1}{(N - m)} \sum_{i=1}^{N-m} B_i^m(r) \tag{10}$$

Similarly, we can calculate each template vector using Equation (11):

$$A_i^m(r) = \frac{1}{(N - m - 1)} \sum_{j=1, j \neq i}^{N-m} \text{number of times that } \mathcal{D}[(AF + 1)(j) - (AF + 1)(i)] < r \tag{11}$$

and summing all template vectors can be calculated using Equation (12):

$$A^m(r) = \frac{1}{(N - m)} \sum_{i=1}^{N-m} A_i^m(r) \tag{12}$$

Finally, *SampEn* can be calculated using Equation (13):

$$SampEn(m, r, N) = -\log \left[\frac{A^m(r)}{B^m(r)} \right] \tag{13}$$

In this study, the values of m , r , etc. were determined based on the multi-scale phenomena of time series confirmed by previous research [4,55].

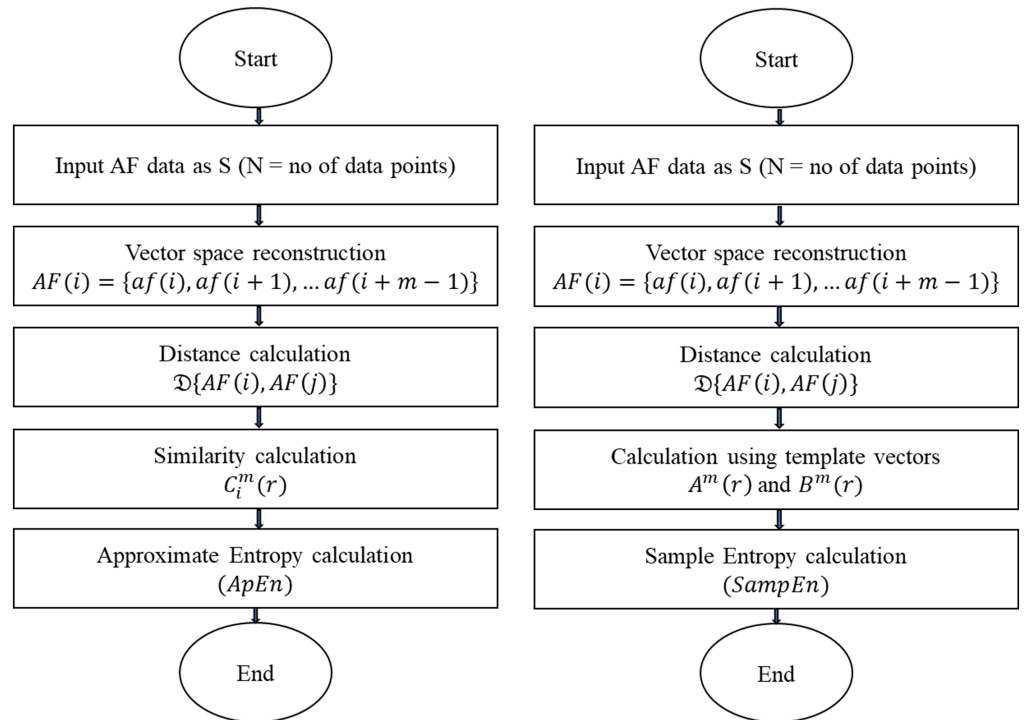


Figure 5. Details of the algorithms to compute Approximate Entropy (*ApEn*) and Sample Entropy (*SampEn*) on AF series.

3.6. Power Spectral Density

The Power Spectral Density (*PSD*) is a measurement of the signal’s intensity or amplitude’s frequency response. In general, it provides a standardized method for describing the distribution of energy in a signal across different frequencies. The *PSD* of $AF(k)$ as a discrete signal $AF(d)$ can be computed as the average magnitude of the Fourier transform squared [4,56], over a time interval and expressed as Equation (14):

$$PSD_{AF(k)} = \left| \frac{1}{2\pi} \sum_{d_1}^{d_2} AF(d) e^{-ikd} \right|^2 = \frac{\widehat{AF}(k) \widehat{AF}_*(k)}{2\pi} \tag{14}$$

where $\widehat{AF}(k)$ is the discrete Fourier transform of $g(d)$ and $\widehat{AF}_*(k)$ is its complex conjugate, and k is the wave number [4,57–59]. We analyzed this *PSD* in the power–law domain across the spatial frequency or wave number k as the Equation (15).

$$PSD_{AF(k)} \sim \frac{1}{k^\beta} \tag{15}$$

where β is the power–law exponent of the *PSD*. We referred to this β as the proxy of planform fluctuations of *AF*, which was computed using the slope of the linear regression fitted to the estimated *PSD* and plotted on log–log scales [4,60]. It is important to note that the entropy described in earlier sections was used to calculate complexity, while power spectral density was used to characterize planform fluctuations of the BR. In other words,

the uniformity of discharge induced by the energy conversion rate of the planform can be measured by the β .

4. Results and Discussion

4.1. Extracted AF and Corresponding PSD of the Brahmaputra River's Planform

AF was generated using the method described in the method sections. We extracted AF, based on the dry season BR planform for each year between 1987 and 2020. Figure 6a illustrates the AF for the seven selected years between 1990 and 2020. The generated AF recreates the dynamic properties commonly observed in the BR's planform.

The PSD of AF was also generated using the procedure outlined in the method section. Figure 6b illustrates the PSD corresponding to the AF depicted in Figure 6a. The best-fitted slope was calculated and used as a measure of fluctuation to be analyzed in the subsequent section.

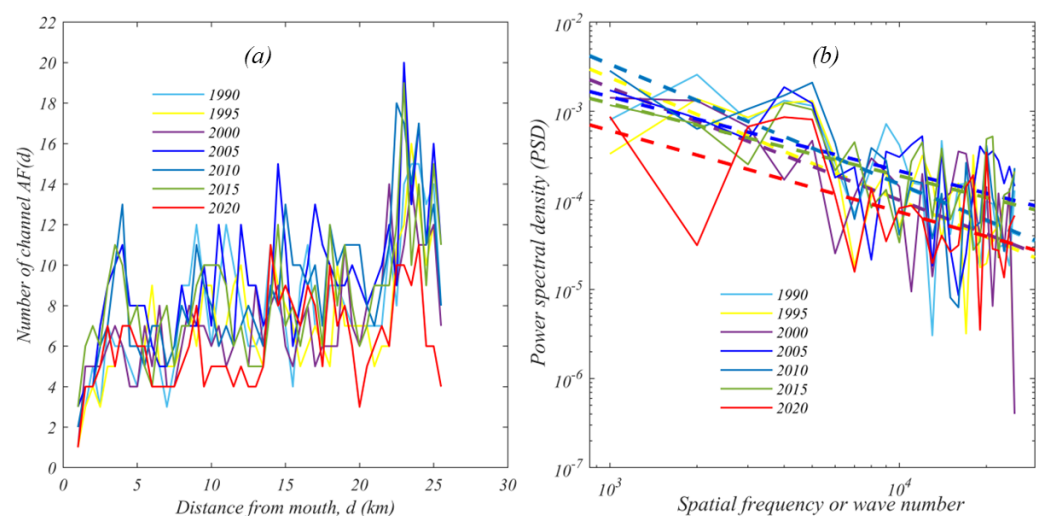


Figure 6. (a) Extracted AF for the BR for the seven selected years and (b) corresponding PSD of AF plotted on a log–log scale.

4.2. Disorder, Complexity and Fluctuation of the Brahmaputra River's Planform

As discussed in an earlier section, $ApEn$ and $SampEn$ represent the disorder and the complexity of the data series, respectively. Consequently, we used $ApEn$ and $SampEn$ to characterize the anastomosing river disorder and complexity nature of the BR. Figure 7a illustrates the BR's yearly value of $ApEn$ and $SampEn$ for the period 1987 to 2020. In addition to having a similar pattern, $ApEn$ and $SampEn$ were significantly linearly correlated with $R^2 \sim 0.17$, and p -value ≤ 0.05 at a 95% confidence interval. Consequently, we may conclude that the possibility of using AF to characterize the BR is enhanced as the complexity of channel patterns grows with disorder or unpredictability. Based on this argument, we expect that a correlation with river dynamic features may exist. To evaluate the dynamic imprint on river planform disorder and complexity, we further investigated the correlation between $ApEn$ and $SampEn$ to the discharge presented in the subsequent section.

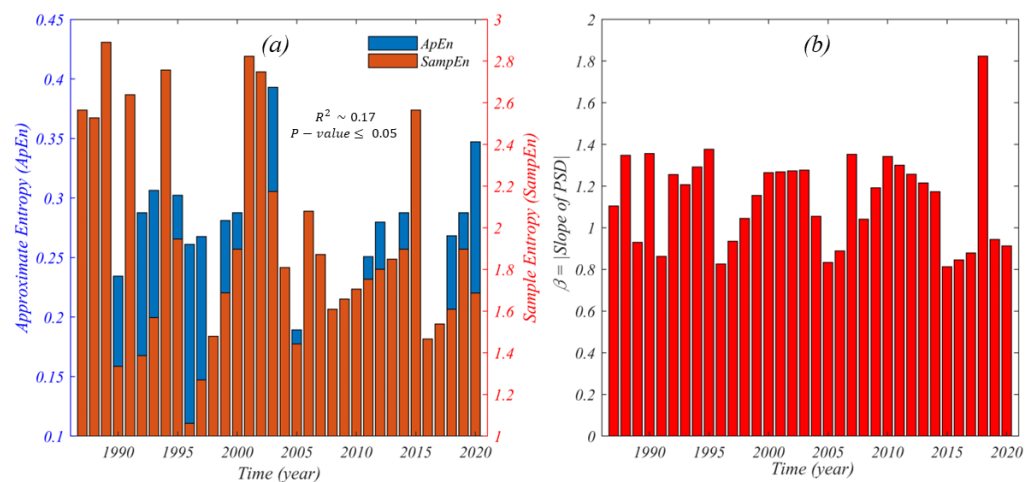


Figure 7. (a) Computed Approximate Entropy ($ApEn$) and Sample Entropy ($SampEn$) on AF series in a bar plot and (b) the corresponding β calculated by fitting the slope to the estimated PSD of AF series plotted on a log–log scale.

In addition to disorder and complexity, the uniformity of energy transfer rate was determined by calculating PSD of AF through $beta$. Figure 7b presents the yearly value of $beta$ for the period from 1987 to 2020. This can be used to describe the nature of the fluctuations of the BR's planform.

4.3. Association between River Discharge and Disorder, Complexity, and Fluctuation

Figure 8a–c exhibits the correlation between $ApEn$ with yearly maximum discharge (Q_{max}), mean yearly wet discharge (Q_{mwet}) and mean yearly dry discharge (Q_{mdry}). It was observed that the value of $ApEn$ increased as the Q_{max} , Q_{mwet} and Q_{mdry} decreased, as shown in Figure 8a–c. It was also observed that Q_{mwet} and Q_{mdry} contributed more to the formation of planform than Q_{max} . Hydraulically, higher discharge transports more sediment from the bed, and potentially widens the main channel [61], thereby reducing the properties of the anastomosing river planform and its complexity. On the other hand, reduced discharge facilitates more sedimentation in the river and formation of bars. The latter process eventually results in oblique flow phenomena that cause a complex network along the riverine landscape and increase complexity. Apart from physical intuition, the correlations between $ApEn$ and discharge values were found to be consistent with the value of $R^2 \sim 0.1$. Although the R^2 value was low, the t -test indicated the presence of significant correlation between $ApEn$ and discharge values within the 95% confidence interval (i.e., $p\text{-value} \leq \sim 0.05$).

Weak correlation was also noticed between observed discharge and $SampEn$ (see Figure 9a–c). However, the t -test indicated significant correlation existed within the 90% confidence interval (i.e., $p\text{-value} \leq \sim 0.1$) for $SampEn$ and the observed discharge. In addition, $SampEn$ was a fairly significantly complex metric in understanding the BR's planform. Therefore, we may conclude that $ApEn$ is a significant and consistent metric to measure the disorder properties of the BR's planform.

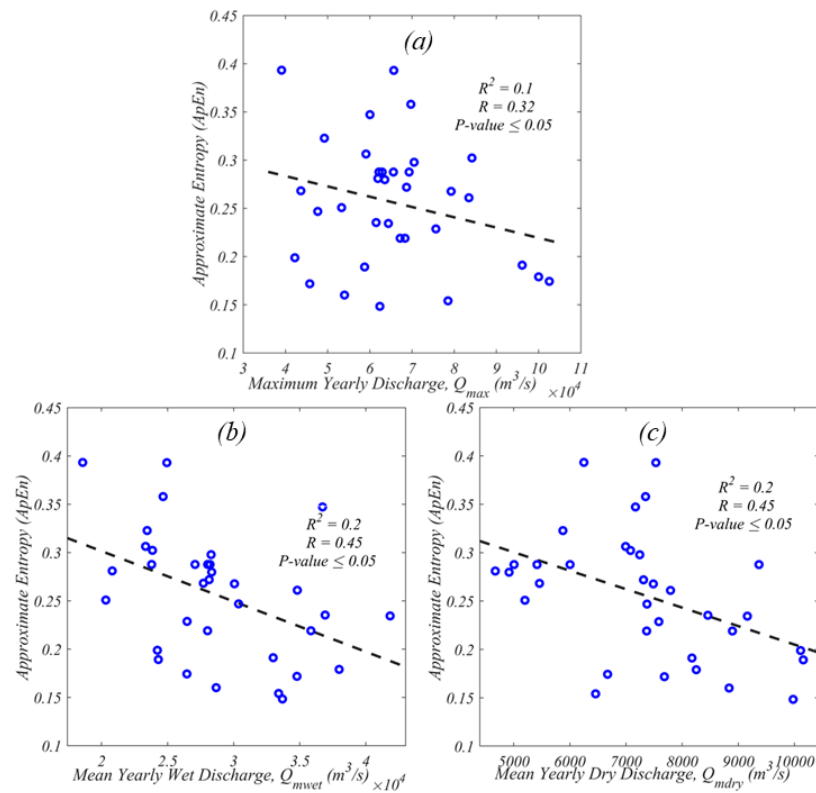


Figure 8. Correlation between Approximate entropy (*ApEn*) and (a) Yearly maximum discharge (Q_{max}), (b) Mean yearly wet discharge (Q_{mwet}) and (c) Mean yearly dry discharge (Q_{mdry}).

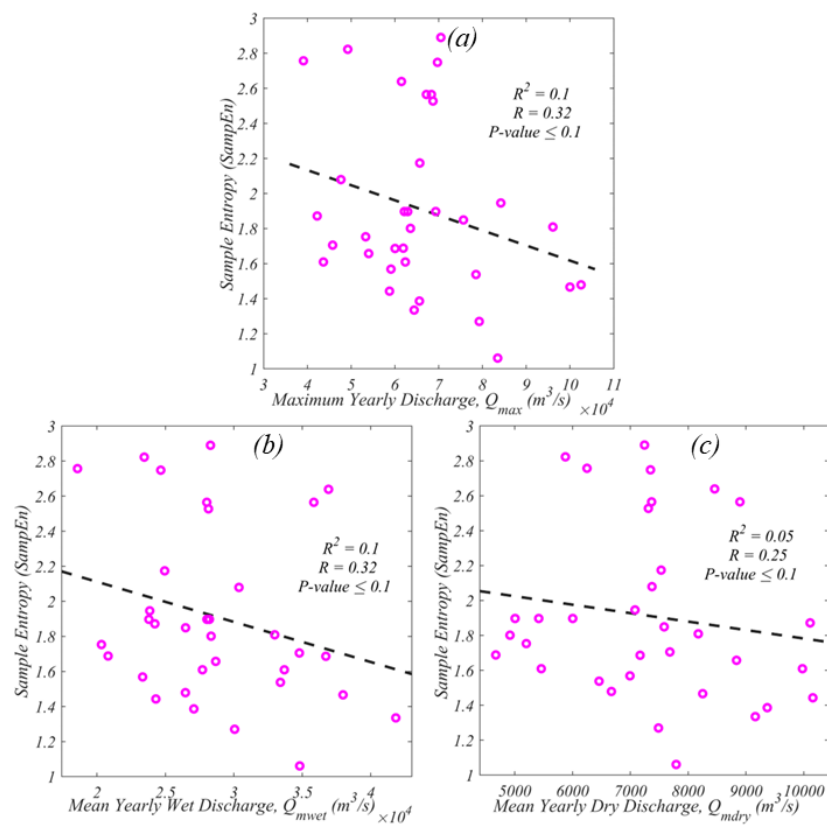


Figure 9. Correlation between Sample Entropy (*SampEn*) and (a) Yearly maximum discharge (Q_{max}), (b) Mean yearly wet discharge (Q_{mwet}) and (c) Mean yearly dry discharge (Q_{mdry}).

Figures 10a–c support our hypothesis that higher discharge results in less fluctuation on the BR’s planform and vice versa. In addition, Q_{mwet} was more responsible for the fluctuation of the planform than Q_{mdry} . Hence, the BR’s planform distributed energy at a non-uniform rate in the case of Q_{mwet} , and vice versa. In other words, the absolute value of the fitted slope of the PSD of AF, plotted on log–log scales, could also reflect fluctuation of the BR’s planform, which was consistent with our disorder and complexity results.

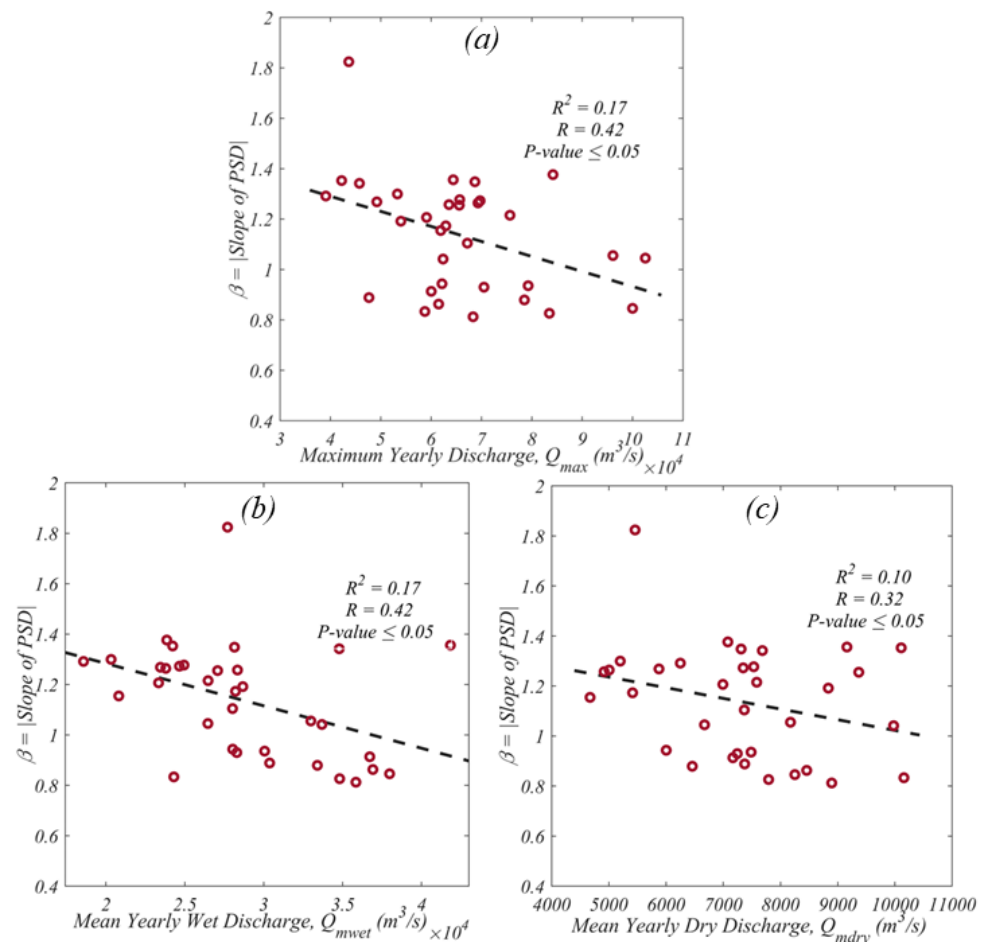


Figure 10. Correlation between β and (a) Yearly maximum discharge (Q_{max}), (b) Mean yearly wet discharge (Q_{mwet}) and (c) Mean yearly dry discharge (Q_{mdry}).

5. Potential Implications Towards Morphological Contexts

Although Leopold and Wolman (1957) proposed a three-part classification of channel planforms (straight, meandering, and braided) [1], there have been a great deal of physical processes responsible for channel changes and the classification of channel planforms. In addition, numerous channel patterns do not fit perfectly within these three categories of classification. In fact, there is higher complexity between meandering and braided categories, as well as within braided categories. As more research is conducted on river systems, new planform types, such as anastomosing, are being identified [62,63].

In this study, we investigated the channel network features of the BR. The AF was considered here as the one-dimensional signal of the two-dimensional channel pattern of the BR, meaning that every change in a channel had the potential to reshape AF. This planform network’s dynamics was influenced, in part, by the evolution of individual bifurcations. We demonstrated the existence of at least one planform property with relevance to fluvial morphodynamics. This innovative characteristic could aid in describing flow curvature and bar dynamics. Hence, it is applicable to different planform networks in the geomorphology of rivers. Our findings indicate that defining a braided river as a network has the potential to

enhance our knowledge of morphodynamics and results in a novel measure of complexity that recognizes the role of a channel as part of the entire planform network system.

6. Conclusions

In this study, a method of representing two-dimensional river planform as a one-dimensional signal is developed, which can be used as an objective metric to quantify planform disorder and complexity and to characterize and explore the anastomosing and planform nature of the Brahmaputra River. We achieved this by implementing a mathematical function, called the Anastomosing Function (*AF*). Additionally, we investigated the concept of entropy along with Power Spectral Density (*PSD*) to quantify the disorder, complexity, and fluctuation of the BR's planforms. The major findings can be summarized as follows:

- The generated and investigated *AF* is capable of accurately transforming a two-dimensional complex network into a one-dimensional spatial signal.
- The Approximate Entropy (*ApEn*) and Sample Entropy (*SampEn*) can be used to quantify the disorder and complexity of river's planforms, respectively, which confirms the reproducibility of the physical features of the river.
- Dynamic imprints, such as yearly maximum discharge (Q_{max}), have significant contributions to the river's planform complexity.
- Q_{max} also showed a significant and consistent contribution to the Brahmaputra River's planform fluctuation.

Overall, our findings reveal the potential use of *AF*, along with the concepts of entropy and *PSD*, to characterize a river under varying geomorphic and climatic conditions. The developed method could be used to quantify the climatic influence (i.e., change of discharge or discharge under extreme events [64]) on planform unpredictability and complexity of the BR. This could be an advantageous tool for engineers and urban planners in implementing sustainable urban development and management around the banks of braided and complex rivers like the BR.

7. Limitations and Recommendations

This study aimed to understand the complexity of the Brahmaputra River (BR) system by utilizing and implementing information theory methods along with the available observed discharge data as one variable to explain the complexity and planform characteristics of the river. The study particularly used discharge data to understand if the response to discharge can be used as a proxy to extreme events on planform complexity. We found that discharge could signal the characteristics of the system and be used as a proxy in understanding planform complexity and geomorphic characteristics of the BR. The river's landscape, which has been experiencing intensive dynamics, the highest population densities and major economic interests, is indeed identified as being the most hydrographically complex and vulnerable area in the world.

Our study is very important to predict planform behavior for rivers that share similar characteristics with the BR. More importantly, our hypotheses were derived from satellite images and based on available discharge data (1987–2020) only. However, planform prediction is a complex phenomenon, requiring numerous hydrological variables and model-predicted outputs, especially to implement integrated water management strategies for braided rivers. While this study proposes a new framework for characterizing planform complexity and the use of observed/historical discharge in understanding the planform complexity of the BR, our method and findings should be used in conjunction with other field observations, hydrological variables, and numerical modeling for better water management and planning implementation. Additionally, although the correlation values between the methods and observed discharges were statistically significant, which led to the conclusion that discharge can be used as one proxy to describe the planform and complexity of the BR, the correlation values were low, which could be partially due to the use of short-term span satellite imagery and discharge data. Given the lack of additional

very long-term data, including long-term observed discharge data, for the study area, we were not able to use additional data and introduce other indicators in characterizing the planform and complexity nature of the BR. Therefore, future work should focus on the use of additional indicators to provide further comprehensive characterization and understanding of the BR's planform and complexity.

Author Contributions: S.S. conducted the research, S.S. and T.S. wrote the initial draft, and analyzed the results. S.U.R. assisted in the data collection. O.T.L., N.A. and I.K. provided feedback on the interpretation of the results. Each author contributed to the manuscript's preparation. All authors have read and agreed to the published version of the manuscript.

Funding: This research received no external funding.

Conflicts of Interest: The authors declare no conflict of interest.

References

1. Leopold, L.B.; Wolman, M.G. *River Channel Patterns: Braided, Meandering, and Straight*; US Government Printing Office: Washington, DC, USA, 1957.
2. Charlton, R. *Fundamentals of Fluvial Geomorphology*; Routledge: London, UK; New York, NY, USA, 2007.
3. Makaske, B. Anastomosing rivers: A review of their classification, origin and sedimentary products. *Earth-Sci. Rev.* **2001**, *53*, 149–196. [[CrossRef](#)]
4. Sarker, S. *Investigating Topologic and Geometric Properties of Synthetic and Natural River Networks under Changing Climate*; University of Central Florida: Orlando, FL, USA, 2021.
5. Sarker, S. Understanding the Complexity and Dynamics of Anastomosing River Planform: A Case Study of Brahmaputra River in Bangladesh. *Earth Space Sci. Open Arch.* **2021**, *1*. [[CrossRef](#)]
6. Sarker, S.; Veremyev, A.; Boginski, V.; Singh, A. Critical nodes in river networks. *Sci. Rep.* **2019**, *9*, 1–11. [[CrossRef](#)] [[PubMed](#)]
7. Khan, I.; Ahammad, M.; Sarker, S. A study on River Bank Erosion of Jamuna River using GIS and Remote Sensing Technology. *Int. J. Eng. Develop. Res.* **2014**, *2*, 3365–3371.
8. Gao, Y.; Sarker, S.; Sarker, T.; Leta, O.T. Analyzing the critical locations in response of constructed and planned dams on the Mekong River Basin for environmental integrity. *Environ. Res. Commun.* **2022**, *4*, 101001. [[CrossRef](#)]
9. Bridge, J.S. The interaction between channel geometry, water flow, sediment transport and deposition in braided rivers. *Geol. Soc.* **1993**, *75*, 13–71. [[CrossRef](#)]
10. Ferguson, R. Understanding braiding processes in gravel-bed rivers: Progress and unsolved problems. *Geol. Soc.* **1993**, *75*, 73–87. [[CrossRef](#)]
11. Klaassen, G.J.; Mosselman, E.; Bruehl, H. *On the Prediction of Planform Changes in Braided Sand-and-Ed Rivers*; Delft Hydraulics: Delft, The Netherlands, 1993.
12. Pradhan, C.; Chembolu, V.; Bharti, R.; Dutta, S. Regulated rivers in India: Research progress and future directions. *ISH J. Hydraul. Eng.* **2021**, 1–13. [[CrossRef](#)]
13. Ashmore, P.E. Laboratory modelling of gravel braided stream morphology. *Earth Surf. Process. Land.* **1982**, *7*, 201–225. [[CrossRef](#)]
14. Ashmore, P.E. How do gravel-bed rivers braid? *Can. J. Earth Sci.* **1991**, *28*, 326–341. [[CrossRef](#)]
15. Ashmore, P. Anabranch confluence kinetics and sedimentation processes in gravel-braided streams. *Geol. Soc.* **1993**, *75*, 129–146. [[CrossRef](#)]
16. Young, W.; Davies, T. Bedload transport processes in a braided gravel-bed river model. *Earth Surf. Process. Land.* **1991**, *16*, 499–511. [[CrossRef](#)]
17. Murray, A.B.; Paola, C. A cellular model of braided rivers. *Nature* **1994**, *371*, 54–57. [[CrossRef](#)]
18. Murray, A.B.; Paola, C. Properties of a cellular braided-stream model. *Earth Surf. Process. Land.* **1997**, *22*, 1001–1025. [[CrossRef](#)]
19. Nykanen, D.K.; Foufoula-Georgiou, E.; Sapozhnikov, V.B. Study of spatial scaling in braided river patterns using synthetic aperture radar imagery. *Water Resour. Res.* **1998**, *34*, 1795–1807. [[CrossRef](#)]
20. Pradhan, C.; Bharti, R.; Dutta, S. Assessment of post-impoundment geomorphic variations along Brahmani River using remote sensing. In Proceedings of the 2017 IEEE International Geoscience and Remote Sensing Symposium (IGARSS), Fort Worth, TX, USA, 23–28 July 2017; pp. 5598–5601.
21. Pradhan, C.; Chembolu, V.; Dutta, S. Impact of river interventions on alluvial channel morphology. *ISH J. Hydraul. Eng.* **2019**, *25*, 87–93. [[CrossRef](#)]
22. Sapozhnikov, V.B.; Foufoula-Georgiou, E. Do the current landscape evolution models show self-organized criticality? *Water Resour. Res.* **1996**, *32*, 1109–1112. [[CrossRef](#)]
23. Sapozhnikov, V.B.; Foufoula-Georgiou, E. Experimental evidence of dynamic scaling and indications of self-organized criticality in braided rivers. *Water Resour. Res.* **1997**, *33*, 1983–1991. [[CrossRef](#)]
24. Walsh, J.; Hicks, D.M. Braided channels: Self-similar or self-affine? *Water Resour. Res.* **2002**, *38*, 1–6. [[CrossRef](#)]
25. Lane, S.N.; Westaway, R.M.; Murray Hicks, D. Estimation of erosion and deposition volumes in a large, gravel-bed, braided river using synoptic remote sensing. *Earth Surf. Process. Land.* **2003**, *28*, 249–271. [[CrossRef](#)]

26. Westaway, R.; Lane, S.; Hicks, D. The development of an automated correction procedure for digital photogrammetry for the study of wide, shallow, gravel-bed rivers. *Earth Surf. Process. Land.* **2000**, *25*, 209–226. [CrossRef]
27. Westaway, R.M.; Lane, S.N.; Hicks, D.M. Remote sensing of clear-water, shallow, gravel-bed rivers using digital photogrammetry. *Photogramm. Eng. Remote Sens.* **2001**, *67*, 1271–1282.
28. Westaway, R.M.; Lane, S.; Hicks, D. Remote survey of large-scale braided, gravel-bed rivers using digital photogrammetry and image analysis. *Int. J. Remote Sens.* **2003**, *24*, 795–815. [CrossRef]
29. Coleman, J.M. Brahmaputra River: channel processes and sedimentation. *Sediment. Geol.* **1969**, *3*, 129–239. [CrossRef]
30. Mosselman, E.; Huisink, M.; Koomen, E.; Seijmonsbergen, A. *Morphological Changes in a Large Braided Sand-Bed River*; John Wiley & Sons: Chichester, UK, 1995.
31. Thorne, C.R.; Russell, A.P.; Alam, M.K. Planform pattern and channel evolution of the Brahmaputra River, Bangladesh. *Geol. Soc.* **1993**, *75*, 257–276. [CrossRef]
32. Goswami, D.C. Brahmaputra River, Assam, India: Physiography, basin denudation, and channel aggradation. *Water Resour. Res.* **1985**, *21*, 959–978. [CrossRef]
33. Sarker, S. Essence of MIKE 21C (FDM Numerical Scheme): Application on the River Morphology of Bangladesh. *Open J. Modell. Simul.* **2022**, *10*, 88–117. [CrossRef]
34. Chembolu, V.; Dutta, S. An entropy based morphological variability assessment of a large braided river. *Earth Surf. Process. Land.* **2018**, *43*, 2889–2896. [CrossRef]
35. Dubey, A.K.; Chembolu, V.; Dutta, S. Utilization of satellite altimetry retrieved river roughness properties in hydraulic flow modelling of braided river system. *Int. J. River Basin Manag.* **2020**, *20*, 1–14. [CrossRef]
36. Karmaker, T.; Medhi, H.; Dutta, S. Study of channel instability in the braided Brahmaputra river using satellite imagery. *Curr. Sci.* **2017**, *112*, 1533–1543. [CrossRef]
37. Sarker, M.H.; Thorne, C.R.; Aktar, M.N.; Ferdous, M.R. Morpho-dynamics of the Brahmaputra–Jamuna river, Bangladesh. *Geomorphology* **2014**, *215*, 45–59. [CrossRef]
38. Valdiya, K. Why does river Brahmaputra remain untamed? *Curr. Sci.* **1999**, *76*, 1301–1305.
39. Dutta, S.; Medhi, H.; Karmaker, T.; Singh, Y.; Prabu, I.; Dutta, U. Probabilistic flood hazard mapping for embankment breaching. *ISH J. Hydraul. Eng.* **2010**, *16*, 15–25. [CrossRef]
40. Nayak, P.; Panda, B. Brahmaputra and the Socio-Economic Life of People of Assam. *The Mahabahu Brahmaputra*; Flood and River Management Agency of Assam: Guwahati, India, 2016; pp. 77–85.
41. Singh, V.; Sharma, N.; Ojha, C.S.P. *The Brahmaputra Basin Water Resources*; Springer Science & Business Media: Berlin/Heidelberg, Germany, 2004; Volume 47.
42. Government of Assam, Water Resources. Brahmaputra River System. Available online: <https://waterresources.assam.gov.in/portlet-innerpage/brahmaputra-river-system> (accessed on 1 October 2021).
43. Marra, W.A.; Kleinhans, M.G.; Addink, E.A. Network concepts to describe channel importance and change in multichannel systems: test results for the Jamuna River, Bangladesh. *Earth Surf. Process. Land.* **2014**, *39*, 766–778. [CrossRef]
44. Fischer, S.; Pietroń, J.; Bring, A.; Thorslund, J.; Jarsjö, J. Present to future sediment transport of the Brahmaputra River: reducing uncertainty in predictions and management. *Region. Env. Change* **2017**, *17*, 515–526. [CrossRef]
45. Sarker, T. Role of Climatic and Non-Climatic Factors on Land Use and Land Cover Change in the Arctic: A Comparative Analysis of Vorkuta and Salekhard. Ph.D. Thesis, The George Washington University, Washington, DC, USA, 2020.
46. Ranjbar, S.; Hooshyar, M.; Singh, A.; Wang, D. Quantifying climatic controls on river network branching structure across scales. *Water Resour. Res.* **2018**, *54*, 7347–7360. [CrossRef]
47. Lashermes, B.; Foufoula-Georgiou, E. Area and width functions of river networks: New results on multifractal properties. *Water Resour. Res.* **2007**, *43*. [CrossRef]
48. Shannon, C.E. A mathematical theory of communication. *Bell Syst. Tech. J.* **1948**, *27*, 379–423. [CrossRef]
49. Delgado-Bonal, A.; Marshak, A. Approximate entropy and sample entropy: A comprehensive tutorial. *Entropy* **2019**, *21*, 541. [CrossRef]
50. Pincus, S.M. Approximate entropy as a measure of system complexity. *Proc. Natl. Acad. Sci. USA* **1991**, *88*, 2297–2301. [CrossRef]
51. Sarker, S.; Sarker, T. Spectral Properties of Water Hammer Wave. *Appl. Mech.* **2022**, *3*, 799–814. [CrossRef]
52. Pincus, S.; Kalman, R.E. Irregularity, volatility, risk, and financial market time series. *Proc. Natl. Acad. Sci. USA* **2004**, *101*, 13709–13714. [CrossRef] [PubMed]
53. Richman, J.S.; Moorman, J.R. Physiological time-series analysis using approximate entropy and sample entropy. *Am. J. Physiol. Heart Circ. Physiol.* **2000**. [CrossRef] [PubMed]
54. Delgado-Bonal, A.; Marshak, A.; Yang, Y.; Holdaway, D. Analyzing changes in the complexity of climate in the last four decades using MERRA-2 radiation data. *Sci. Rep.* **2020**, *10*, 1–8. [CrossRef]
55. Ranjbar, S.; Singh, A. Entropy and intermittency of river bed elevation fluctuations. *J. Geophys. Res. Earth Surf.* **2020**, *125*, e2019JF005499. [CrossRef]
56. Sarker, S. A Story on the Wave Spectral Properties of Water Hammer. *enrXiv* **2021**. [CrossRef]
57. Stoica, P.; Moses, R.L. *Spectral Analysis of Signals*; Pearson and Prentice Hall: Upper Saddle River, NJ, USA, 2005.
58. Stull, R.B. *An Introduction to Boundary Layer Meteorology*; Springer Science & Business Media: Berlin/Heidelberg, Germany, 2012; Volume 13.

59. Gardner, W.A.; Robinson, E.A. *Statistical Spectral Analysis—A Nonprobabilistic Theory*; Prentice-Hall Inc.: Upper Saddle River, NJ, USA, 1989.
60. Pilgram, B.; Kaplan, D.T. A comparison of estimators for 1f noise. *Phys. D Nonlin. Phen.* **1998**, *114*, 108–122. [[CrossRef](#)]
61. Sarker, S. A Short Review on Computational Hydraulics in the context of Water Resources Engineering. *Open J. Modell. Simul.* **2022**, *10*, 1–31. [[CrossRef](#)]
62. Smith, D.G.; Smith, N.D. Sedimentation in anastomosed river systems; examples from alluvial valleys near Banff, Alberta. *J. Sediment. Res.* **1980**, *50*, 157–164. [[CrossRef](#)]
63. David Knighton, A.; Nanson, G.C. Anastomosis and the continuum of channel pattern. *Earth Surf. Process. Land.* **1993**, *18*, 613–625. [[CrossRef](#)]
64. Sarker, S. Fundamentals of Climatology for Engineers: Lecture Note. *Eng* **2022**, *3*, 573–595. [[CrossRef](#)]

Disclaimer/Publisher’s Note: The statements, opinions and data contained in all publications are solely those of the individual author(s) and contributor(s) and not of MDPI and/or the editor(s). MDPI and/or the editor(s) disclaim responsibility for any injury to people or property resulting from any ideas, methods, instructions or products referred to in the content.